Editors' Suggestion | Featured in Physics

Revisiting the Phase Diagram of Methane

Mengnan Wang,[1,2] Miriam Peña-Alvarez,[1,*] Ross T. Howie,[1,3] and Eugene Gregoryanz[3,4,1,5,†]

[1]Centre for Science at Extreme Conditions and School of Physics and Astronomy, University of Edinburgh, Edinburgh, United Kingdom
[2]Department of Earth and Planetary Sciences, Stanford University, Stanford, California, USA
[3]Center for High Pressure Science and Technology Advanced Research, Shanghai, People's Republic of China
[4]Shanghai Advanced Research in Physical Sciences, Shanghai, People's Republic of China
[5]Key Laboratory of Materials Physics, Institute of Solid State Physics, Chinese Academy of Science, Hefei, People's Republic of China

(Received 29 May 2025; accepted 20 November 2025; published 26 January 2026)

Combination of optical spectroscopy and *in situ* high-temperature–high-pressure techniques, were employed to investigate the melting curve and map out the location of methane's solid phases up to 45 GPa and 1100 K. The experiments yield two distinct diagrams, one that demonstrates the kinetic phase transformations and the other presenting the equilibrium states usually reached with time. Raman spectroscopy demonstrates that the appearance and transitions between the higher pressure phases (VII, VIII, and IX) are strongly dependent on the pressure-temperature-time path. Combined visual observations and Raman spectroscopy indicate that the melting curve of methane extends to significantly higher temperatures than previously reported, e.g., ∼1000 K at 15 GPa. The study also suggests that some inconsistencies in the earlier melting data could be attributed to photochemical dissociation and/or a reaction induced by high-intensity light sources.

DOI: 10.1103/7hxd-hhjf

Because of the deceptive simplicity of its molecule and being the main constituent of natural gas found on Earth, methane is a textbook example of a chemical compound that is important in fundamental and environmental sciences as well as in industry [1–13]. Because methane molecules have closed electron shells and are almost spherically symmetric, methane has some physical properties similar to those of rare gases such as argon. Upon solidification, methane forms a van der Waals molecular solid with a cubic fcc lattice (phase I) [14]. However, the molecular nature of crystalline methane presents particular interest because it belongs to a class of materials where the constituent molecules are orientationally disordered over a wide pressure-temperature range. Unlike rare gas solids, which have rather simple phase diagrams, with a maximum of two known phases (fcc and hcp) [15,16], methane is claimed to have nine [17,18].

Below 300 K the phase diagram of methane has been mainly investigated by infrared and Raman spectroscopy [17,19], while the structural characterization information was derived from x-ray and neutron diffraction at room temperature [18,20–22]. Surprisingly, despite methane's geophysical and planetary significance, the high-temperature and high-pressure phase data remain rather limited [6,23–27]. Early studies determined the melting curve up to 4.8 GPa by observing discontinuity in the pressure-temperature curve caused by the volume change during melting [23]. The subsequent work extended this to around 7 GPa based on the visual observations of morphological changes of the samples [25], while the laser-heating study presented the essentially horizontal melting curve up to 80 GPa [24]. Subsequently, laser heating experiments, combined with Raman spectroscopy of quenched samples, produced the current phase diagram of methane up 80 GPa and 2200 K [6]. However, besides the reliance on measurements from quenched products, the latter study presented the melting curve [6], which showed the discrepancies with the published data at pressures as low as 5 GPa [25]. The phase diagram presented the estimated error bars reaching 30%–40% of the claimed temperatures while placing the tentative vertical lines to mark the room temperature solid-solid phase transition lines [6]. Given this ambiguity and other discrepancies in the locations of the phases at high pressures [28], further experiments aimed at fully mapping the high-temperature phase diagram of methane are highly desirable.

In this Letter, we present optical spectroscopic studies of dense methane, conducted in a diamond anvil cell up to 45 GPa, combined with *in situ* resistive heating to 1100 K. The evolution of Raman modes across phase transitions between I, VII, VIII, IX, and the fluid phase was tracked.

*Contact author: miriam.pena.alvarz@ed.ac.uk
†Contact author: e.gregoryanz@sharps.ac.cn

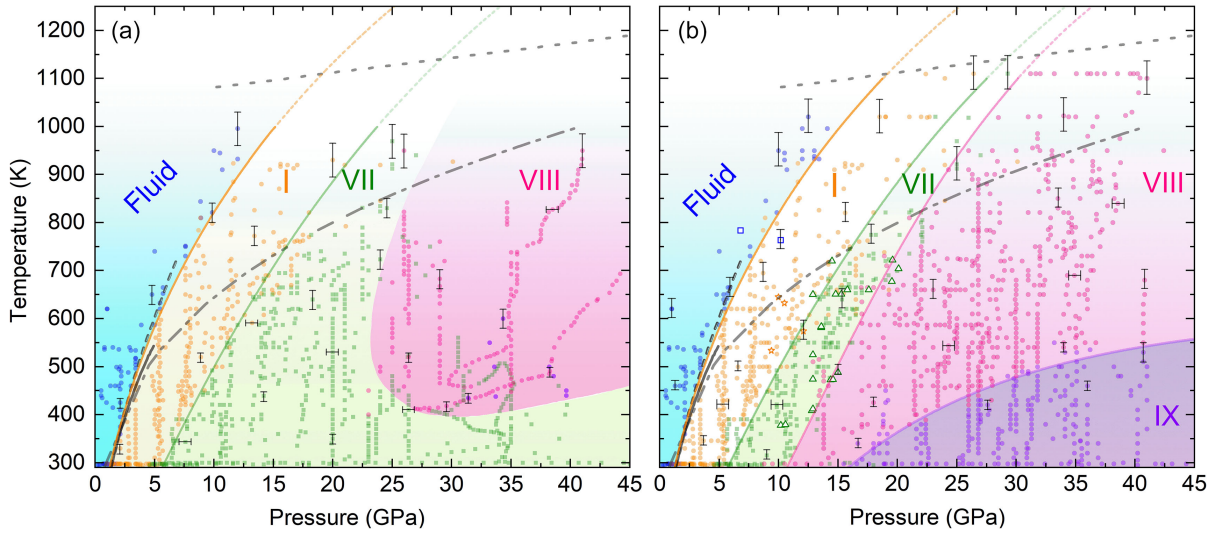

FIG. 1. (a) Transformation diagram of methane. (b) Equilibrium diagram of methane. The colored, solid circles represent the different the *P-T* points where the Raman spectra were collected during heating and isothermal decompression experiments. The color code is used as follows: dark blue for CH_4 fluid state, orange for phase I, green for phase VII, pink for phase VIII, purple for phase IX. Empty symbols denote measurements obtained via synchrotron x-ray diffraction. The colored solid lines indicate experimentally determined phase boundaries measured in this Letter and the dashed color lines are their extrapolations. The gray solid line corresponds to the melting boundary reported by [23], the dashed gray line to [24], the solid gray line to [25], and the dot-dashed line to the melting curve from [6]. Representative error bars are shown for some of the points in order not to overload the figures.

Raman spectroscopy reveals that, above 10 GPa, methane's phase behavior is governed by kinetic effects across a broad *P-T* range. The phase boundaries between the fluid and phases I, VII, and VIII display similarly steep positive slopes, suggesting density-driven transitions, whereas the much shallower slope between phases VIII and IX indicates a transition predominantly driven by entropy. The melting curve, determined by observing morphological changes and monitoring the corresponding changes in Raman spectra appears to be significantly higher than previously reported from laser-heating methods. Furthermore, methane photolysis is not inhibited under exposure to intense light, thereby affecting the expected temperature-induced decomposition. These elevated melting temperatures, in combination with kinetic control and light-induced reactivity, underscore that simple extrapolations are inadequate for predicting methane's behavior under planetary conditions.

For the experimental details, description of the setups, data treatment, and additional figures, the reader is referred to Supplemental Material [29], which includes Refs. [8,30–39]. The combined results from all experiments (more than 70) are summarized in Fig. 1. Phase transitions were identified using established Raman spectroscopy criteria, specifically by evaluating pressure- and temperature-induced changes in the C-H stretching modes ν_1 and ν_3 [19,22,28,40,41], and crossed-checked with visual observations and x-ray diffraction for melting; see Supplemental Material, Figs. S1–S5 [29]. In different works, methane phases are labeled as numbers or letters [40]; in this Letter, we adopt an original numerical labeling system referring to phase A as VII, B as VIII and HP as IX.

We find that fluid CH_4 solidifies into phase I (fcc) [14] at any *P-T* conditions when the melting curve is crossed (Figs. 1 and 2 and Figs. S4 and S5 [29]). Upon isothermal compression, phase I directly transforms into the complex

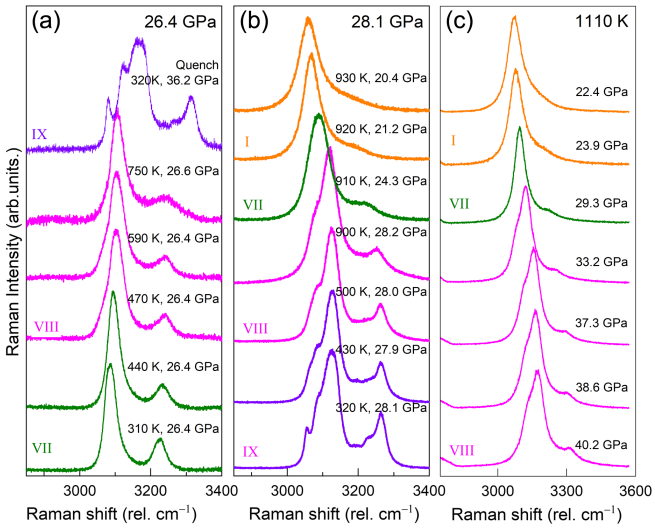

FIG. 2. (a) Isobaric heating up to 750 K from 26.4 GPa, followed by quenching. (b) Quasi-isobaric heating up to 930 K from 28.1 GPa. (c) Isothermal decompression from 40.2 GPa at 1110 K. Different colors indicate distinct CH_4 phases: orange for phase I, green for phase VII, pink for phase VIII, and purple for phase IX.

rhombohedral phase VII, in a wide temperature range [21] [Figs. 1 and 2(a) and Figs. S4 and S5 [29]]. Our results demonstrate that phase I is thermodynamically stable as its transitions to both the liquid state and phase VII are fully reversible and independent of P-T paths and timescales. In contrast, when phase VII is compressed at room temperature over durations ranging from minutes to several hours, it can be "trapped" [6,17,19,22,41] even at pressures exceeding 100 GPa (Fig. S4 [29]). This (meta)stable persistence of phase VII at room temperature is consistent with previous observations in which methane was pressurized up to 165 GPa [42], but it contradicts other phase diagrams reporting phases VIII and IX between 8 and 25 GPa [6,17,19,22,41].

Figure 1(a) shows a transformation-controlled diagram that does not account for any time-dependent effects, thereby suppressing the sluggish VII → VIII transition. Under these conditions, phase VII appears stable across an extended P-T range, where phases VIII and IX are observed [18,22]. Notably, phase VIII (complex α-Mn cubic structure, with 58 molecules per unit cell and space group $I\bar{4}3m$) and phase IX (rhombohedral $R3$ symmetry with a unit cell containing 87 molecules) structurally are more complex than phase VII and appear to be positioned above phase VII in this kinetic picture, a physically implausible configuration that underscores the nonequilibrium nature of the observed phase relation [18,22]. Upon heating, phases VII and VIII irreversibly transform into their respective equilibrium forms. For example, our results show that below 20 GPa, even at temperatures up to 660 K, the sample remains trapped in phase VII, see Fig. S6 [29]. In contrast, when phase VII is heated isobarically above 22 GPa to temperatures exceeding 400 K, the transition to phase VIII occurs instantaneously (Fig. S6 [29]). If pressure is released at high temperature, phase VIII reversibly transforms back to phase VII. However, upon cooling to room temperature, phase VIII does not revert to phase VII but instead transitions to another phase, IX [Fig. 2(a)]. Together, these observations suggest that this picture reflects a transformation sequence governed by kinetic trapping and metastability, rather than true equilibrium phase boundaries.

To reconcile the observed discrepancies in the appearance of the phases (see above and [6,17,19,22,41]), we have included time as parameter in our measurements. Our "time-dependent" or, more accurately, "equilibrium" experiments involved gradually increasing pressure from 8 to 25 GPa. The sample was allowed to reach equilibrium over periods ranging from several days to months, while its state was continuously monitored using Raman spectroscopy. To promote phase transformations, temperature cycling was also performed at various pressures. Figure 1(b) illustrates the equilibrium behavior when heating was initiated from a thermodynamically stable phase. Here, a reproducible sequence of temperature-driven transitions is observed: IX → VIII → VII → I → fluid, occurring at both room and elevated temperatures. In Fig. 2(b), after slowly increasing pressure above 16 GPa at 300 K, phase IX was reached. Subsequent heating from 28 GPa revealed the same transition sequence: IX → VIII → VII → I transitions. The phase transition sequence has been confirmed through multiple isobaric heating and isothermal compression and decompression experiments [Fig. 2(c) and Supplemental Material, Figs. S7 and S8 [29]], enabling precise mapping of the high P-T phase lines between the fluid, phases I, VII, VIII, and IX. Interestingly, upon isobaric heating of phase IX, phase VIII emerges back at high temperature and higher pressures as represented in Fig. 1(b), e.g., at 17 GPa and 374 K, 13 GPa and 350 K, 22 GPa and 400 K, 28 GPa and 500 K; see also Fig. S7 [29]. The transformation between VIII and IX is reversible along the entire phase boundary. Notably, neither the previously reported α phase nor the HP2 phase was observed in any of our equilibrium measurements, despite following similar time-dependent pathways [6,24,28]. We note that, in the equilibrium phase diagram, Fig. 1(b), the phase boundaries between the fluid, phases I, VII, and VIII exhibit similar steep positive slopes with respect to pressure, which runs nearly parallel to one another, suggesting the standard density-driven phase transitions. Each successive phase adopts a more complex structure than its predecessor, a scenario similar to that observed in N_2; see, for example, Ref. [43]. In contrast, the boundary between phases VIII and IX has a significantly shallower slope, nearly parallel to the pressure axis above 30 GPa in P-T space, suggesting an entropy-driven transition between VIII and IX, which is not very common behavior. This shallow boundary between phases VIII and IX is analogous to the phase I to II and III to IV transitions in dense H_2, with both phase II and IV being governed by the quantum effects [31,44–46].

In this Letter, we systematically investigated the methane melting curve using Raman spectroscopy correlated with visual observations. For example, during heating at 11 GPa from phase VII, Figs. 3(a) and 3(b), we observe a distinct discontinuity in the full width at half maximum (FWHM) and Raman shift of ν_1 between 548 and 576 K, accompanied by a decrease in intensity of ν_1 (see Fig. S9 [29] for spectral analysis). These spectral changes are characteristic of the transition to phase I, as further supported by our synchrotron x-ray diffraction measurements (see Fig. S3). Visually, phase VII exhibits a granular texture that upon further heating and consequent transitioning to phase I anneals into well-defined large crystals. As shown in Fig. 3(a), the crystal boundaries progressively sharpen and become better defined, consistent with the previous reports for phase VII [21]. Further heating beyond 920 K results in the disappearance of crystal boundaries, accompanied by the sinking of the $Sm:SrB_4O_7$ chip, see

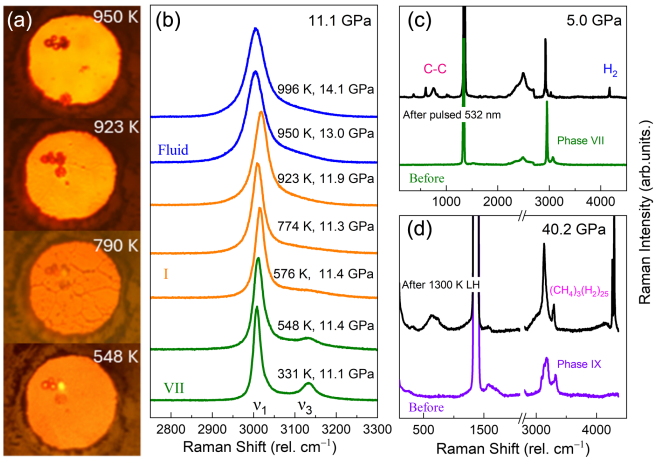

FIG. 3. (a). Photomicrographs of methane solids and fluid at different temperatures during heating experiment. (b) Raman spectra of CH_4 showing the C-H stretching modes ν_1 and ν_3 during resistive heating up to 996 K from 11.1 GPa. (c) Raman spectrum before and after the sample was exposed to the intense pulsed 532 nm radiation, with both pure C and H_2 present [6]. (d) Raman spectrum before and after IR laser heating up to ~1300 K at 40.2 GPa from phase IX, with H_2 release and the formation of the van der Waals compound $(CH_4)_3(H_2)_{25}$ [47].

Fig. 3. This observation aligns very well with the spectral changes, where the FWHM of ν_1 increases discontinuously and shows a pronounced downshift during the phase I–fluid transition. Independent x-ray diffraction data further confirm the assignment of melting under these conditions. Additional spectral analyses at different pressures further support this assignment and are provided in Figs. S10 and S11 in Supplemental Material [29]. Notably, our observed melting temperatures in this Letter are approximately 25%–30% higher than previously reported (e.g., ~1000 K at 50 GPa [6]), yet still significantly lower than the estimated isentropes of giant gas planets.

Melting studies of dense methane have suggested pathways leading to oligomer formation (e.g., complex prebiotic molecules) or decomposition into hydrogen and diamond processes considered essential to planetary dynamics [6,24,48,49]. We observed solid phases in regions where decomposition was previously reported, suggesting a potential role for light-induced chemistry. Given methane's well-characterized photochemical sensitivity [50,51], we hypothesize that intense light exposure can drive solid-phase transformations and chemical decomposition. We also note that, even if the mildly elevated temperatures alone can lead to the formation of methane from C and H_2 [8], one can expect that the combination of temperature and intense light, particularly within the vicinity of melting, can cause dissociation and/or other chemical reactions. In one of the experiments, we observed pure hydrogen after the sample was irradiated with the pulsed intense light of 532 nm for 1 s at 300 K and 5.0 GPa, Fig. 3(c), while in fluid (< 1 GPa) methane decomposed within 1 sec under pulsed supercontinuum illumination, also producing detectable H_2 signals (Fig. S12 [29]). At 3.6 and 5.6 GPa, the longer exposures (1–3 h) led to sample darkening and the emergence of a Raman band at 1600 cm^{-1}, indicative of sp^2-bonded carbon. At 16 GPa, extended irradiation (12 h) produced increased background fluorescence and a distinct Raman peak at 751 cm^{-1}, possibly arising from C-H bending in larger hydrocarbons, C-C coupled vibrations, or defect-induced features in disordered carbon. Similarly, at 40 GPa, laser heating led to decomposition, reinforcing the role of high-intensity light and temperature in driving chemical changes even under extreme compression [Fig. 3(d)]. These observations underscore the complex interplay of pressure, temperature, and light in governing methane's chemical behavior, with important implications for both high-pressure laboratory studies and chemical evolution in methane-rich planetary interiors.

In summary, combined optical spectroscopy across an extended pressure-temperature range reveals both the transformation and equilibrium phase diagrams of methane, characterized by a uniquely layered structure. Above 10 GPa, its phase behavior is dominated by kinetics and metastability. The melting curve extends to significantly higher temperatures than previously reported. Methane's sensitivity to high-intensity light suggests that laser-induced photochemistry may have influenced earlier high-pressure results [6,24,48,49], complicating the distinction between thermal and nonthermal effects. These findings carry important implications for methane-rich planetary interiors, where extreme conditions may trigger unexpected chemical reactions.

Acknowledgments—M. W. acknowledges support from the Principal's Career Development Scholarship at the University of Edinburgh. The work was supported by the UKRI Future Leaders fellowship No. Mrc-Mr/T043733/1 and the European Research Council (ERC) under the European Union's Horizon 2020 research and innovation program (Grant Agreement No. 948895, MetElOne). The authors thank Ms. Hannah A. Shuttleworth, Dr. Mikhail A. Kuzovnikov, and Dr. Tomas Marqueño for assistance during x-ray experiments and Dr. John Proctor for providing us with pressure calibrants. We would also like to thank Dr. Konstantin Glazyrin for assistance. We acknowledge DESY (Hamburg, Germany), a member of the Helmholtz Association HGF, for the provision of experimental facilities. Parts of this research were carried out at PETRA-III P02.2.

Data availability—The data are not publicly available. The data are available from the authors upon reasonable request.

[1] D. C. Catling, K. J. Zahnle, and C. P. McKay, Science **293**, 839 (2001).
[2] J. L. Atwood, L. J. Barbour, and A. Jerga, Science **296**, 2367 (2002).
[3] V. Formisano, S. Atreya, T. Encrenaz, N. Ignatiev, and M. Giuranna, Science **306**, 1758 (2004).
[4] A. E. Dekas, R. S. Poretsky, and V. J. Orphan, Science **326**, 422 (2009).
[5] C. J. Sapart, G. Monteil, M. Prokopiou, R. S. W. van de Wal, J. O. Kaplan, P. Sperlich, K. M. Krumhardt, C. van der Veen, S. Houweling, M. C. Krol *et al.*, Nature (London) **490**, 85 (2012).
[6] S. S. Lobanov, P.-N. Chen, X.-J. Chen, C.-S. Zha, K. D. Litasov, H.-K. Mao, and A. F. Goncharov, Nat. Commun. **4**, 2446 (2013).
[7] H. Schmiedt, P. Jensen, and S. Schlemmer, Phys. Rev. Lett. **117**, 223002 (2016).
[8] M. Peña-Alvarez, A. V. Brovarone, M.-E. Donnelly, M. Wang, P. Dalladay-Simpson, R. Howie, and E. Gregoryanz, Nat. Commun. **12**, 6387 (2021).
[9] W. Huang, A. C. Johnston-Peck, T. Wolter, W.-C. D. Yang, L. Xu, J. Oh, B. A. Reeves, C. Zhou, M. E. Holtz, A. A. Herzing *et al.*, Science **373**, 1518 (2021).
[10] J. D. Maasakkers, D. J. Varon, A. Elfarsdóttir, J. McKeever, D. Jervis, G. Mahapatra, S. Pandey, A. Lorente, T. Borsdorff, L. R. Foorthuis *et al.*, Sci. Adv. **8**, eabn9683 (2022).
[11] E. Ridente, D. Hait, E. A. Haugen, A. D. Ross, D. M. Neumark, M. Head-Gordon, and S. R. Leone, Science **380**, 713 (2023).
[12] L. Shen, D. J. Jacob, R. Gautam, M. Omara, T. R. Scarpelli, A. Lorente, D. Zavala-Araiza, X. Lu, Z. Chen, and J. Lin, Nat. Commun. **14**, 4948 (2023).
[13] B. Shirizadeh, M. Villavicencio, S. Douguet, J. Trüby, C. Bou Issa, G. S. Seck, V. D'herbemont, E. Hache, L.-M. Malbec, J. Sabathier *et al.*, Nat. Commun. **14**, 5756 (2023).
[14] R. M. Hazen, H.-K. Mao, L. W. Finger, and P. M. Bell, Appl. Phys. Lett. **37**, 288 (1980).
[15] H. Cynn, C.-S. Yoo, B. Baer, V. Iota-Herbei, A. K. McMahan, M. Nicol, and S. Carlson, Phys. Rev. Lett. **86**, 4552 (2001).
[16] H. Shimizu, M. Kawajiri, T. Kume, S. Sasaki, Y. A. Freiman, and S. M. Tretyak, Phys. Rev. B **79**, 132101 (2009).
[17] R. Bini, L. Ulivi, H. J. Jodl, and P. R. Salvi, J. Chem. Phys. **103**, 1353 (1995).
[18] H. E. Maynard-Casely, L. F. Lundegaard, I. Loa, M. I. McMahon, E. Gregoryanz, R. J. Nelmes, and J. S. Loveday, J. Chem. Phys. **141**, 234313 (2014).
[19] R. Bini and G. Pratesi, Phys. Rev. B **55**, 14800 (1997).
[20] L. Sun, W. Yi, L. Wang, J. Shu, S. Sinogeikin, Y. Meng, G. Shen, L. Bai, Y. Li, J. Liu, H.-K. Mao, and W. L. Mao, Chem. Phys. Lett. **473**, 72 (2009).
[21] H. E. Maynard-Casely, C. L. Bull, M. Guthrie, I. Loa, M. I. McMahon, E. Gregoryanz, and J. S. Loveday, J. Chem. Phys. **133**, 064504 (2010).
[22] M. Bykov, E. Bykova, C. J. Pickard, M. Martinez-Canales, K. Glazyrin, J. S. Smith, and A. F. Goncharov, Phys. Rev. B **104**, 184105 (2021).
[23] T. Yagi and H. Suzuki, Proc. Jpn. Acad. Ser. B **66**, 167 (1990).
[24] H. Hirai, K. Konagai, T. Kawamura, Y. Yamamoto, and T. Yagi, Phys. Earth Planet. Inter. **174**, 242 (2009).
[25] E. H. Abramson, High Press. Res. **31**, 549 (2011).
[26] L. J. Conway and A. Hermann, Geosciences **9**, 227 (2019).
[27] A. S. Naumova, S. V. Lepeshkin, and A. R. Oganov, J. Phys. Chem. C **123**, 20497 (2019).
[28] P.-N. Chen, C.-S. Zha, X.-J. Chen, J. Shu, R. J. Hemley, and H.-K. Mao, Phys. Rev. B **84**, 104110 (2011).
[29] See Supplemental Material at http://link.aps.org/supplemental/10.1103/7hxd-hhjf for the experimental details, description of the setups, data treatment, and additional figures, which includes Refs. [8,30–39].
[30] Y. Akahama and H. Kawamura, J. Appl. Phys. **100**, 043516 (2006).
[31] R. T. Howie, P. Dalladay-Simpson, and E. Gregoryanz, Nat. Mater. **14**, 495 (2015).
[32] E. Gregoryanz, A. F. Goncharov, K. Matsuishi, H.-K. Mao, and R. J. Hemley, Phys. Rev. Lett. **90**, 175701 (2003).
[33] M. Peña-Alvarez, P. Dalladay-Simpson, X.-D. Liu, V. Afonina, H.-C. Zhang, R. T. Howie, and E. Gregoryanz, J. Appl. Phys. **125**, 025901 (2019).
[34] A. Zerr, G. Serghiou, R. Boehler, and M. Ross, High Press. Res. **26**, 23 (2006).
[35] G. Shen, M. L. Rivers, Y. Wang, and S. R. Sutton, Rev. Sci. Instrum. **72**, 1273 (2001).
[36] R. A. Fischer, A. J. Campbell, O. T. Lord, G. A. Shofner, P. Dera, and V. B. Prakapenka, Geophys. Res. Lett. **38**, L24301 (2011).
[37] H.-P. Liermann, Z. Konôpková, W. Morgenroth, K. Glazyrin, J. Bednarčik, E. E. McBride, C. Prescher, V. B. Prakapenka, A. Makhluf, M. Wiencek, and H. Franz, J. Synchrotron Radiat. **22**, 908 (2015).
[38] C. Prescher and V. B. Prakapenka, High Press. Res. **35**, 223 (2015).
[39] W. Kraus and G. Nolze, J. Appl. Crystallogr. **29**, 301 (1996).
[40] Y. H. Wu, S. Sasaki, and H. Shimizu, J. Raman Spectrosc. **26**, 963 (1995).
[41] H. Hirai, K. Konagai, T. Kawamura, Y. Yamamoto, and T. Yagi, Chem. Phys. Lett. **454**, 212 (2008).
[42] J. E. Proctor, H. E. Maynard-Casely, M. A. Hakeem, and D. Cantiah, J. Raman Spectrosc. **48**, 1777 (2017).
[43] E. Gregoryanz, A. F. Goncharov, R. J. Hemley, and H.-K. Mao, Phys. Rev. B **66**, 224108 (2002).
[44] P. Dalladay-Simpson, R. T. Howie, and E. Gregoryanz, Nature (London) **529**, 63 (2016).
[45] X.-D. Liu, R. T. Howie, H.-C. Zhang, X.-J. Chen, and E. Gregoryanz, Phys. Rev. Lett. **119**, 065301 (2017).
[46] H. Xu, W. Xu, P. Wang, L. Liu, X.-D. Liu, and E. Gregoryanz, Phys. Rev. B **111**, 024109 (2025).
[47] U. Ranieri, L. J. Conway, M.-E. Donnelly, H. Hu, M. Wang, P. Dalladay-Simpson, M. Peña-Alvarez, E. Gregoryanz,

A. Hermann, and R. T. Howie, Phys. Rev. Lett. **128**, 215702 (2022).
[48] L. R. Benedetti, J. H. Nguyen, W. A. Caldwell, H. Liu, M. Kruger, and R. Jeanloz, Science **286**, 100 (1999).
[49] M. Frost, R. S. McWilliams, E. Bykova, M. Bykov, R. J. Husband, L. M. Andriambariarijaona, S. Khandarkhaeva, B. Massani, K. Appel, C. Baehtz *et al.*, Nat. Astron. **8**, 174 (2024).
[50] D. F. Strobel, J. Atmos. Sci. **26**, 906 (1969).
[51] J. F. Kasting, K. J. Zahnle, and J. C. G. Walker, Precambrian Res. **20**, 121 (1983).